Dynamical effects on the de-excitation of hot nuclei with $A \simeq 160$

M. Gonin, L. Cooke, K. Hagel, Y. Lou, J. B. Natowitz, R. P. Schmitt, S. Shlomo, B. Srivastava, W. Turmel, H. Utsunomiya, and R. Wada
Cyclotron Istitute, Texas A&M University, College Station, Texas 77843

G. Nardelli, G. Nebbia, G. Viesti, and R. Zanon
Istituto Nazionale di Fisica Nucleare, Sezione di Padova, I-35131, Padova, Italy

B. Fornal and G. Prete
Istituto Nazionale di Fisica Nucleare, Laboratori Nazionali Legnaro, I-35020, Legnaro, Italy

K. Niita and S. Hannuschke
Institut für Theoretische Physik, Universität Giessen, 6300 Giessen, West Germany

P. Gonthier
Department of Physics, Hope College, Holland, Michigan 49423

B. Wilkins
Chemistry Division, Argonne National Laboratory, Argonne, Illinois 60439
(Received 4 April 1990)

Light charged-particle emission and neutron emission have been measured for the fusion-evaporation and fusion-fission channels in the $^{60}Ni + ^{100}Mo$ reaction at 550 and 655 MeV bombarding energies. Temperatures, emission barriers, and multiplicities for the particles detected in coincidence with evaporation residues and fission fragments have been determined. For the evaporation residue data, the "first-chance" spectra of particles emitted from the compound nucleus have been isolated and the same initial temperature for the different evaporated particles has been extracted. The inverse level density parameter $K = A/a$ reaches a value of 13.8 ± 0.7 MeV at $E_{th} \simeq 236$ MeV. A decrease of the apparent emission barriers for the charged-particle emission at high excitation energy suggests dynamical effects on the de-excitation process. Analysis of the fissionlike events shows a saturation of light particle emission from the fission fragments. Using the average energies and multiplicities of the emitted neutrons, and charged particles, it has been found that for both initial excitation energies, 251 and 293 MeV, scission occurs at an excitation energy $\simeq 140$ MeV. For both fusion evaporation and fusion fission, the light charged particles are preferentially emitted during the early part of the de-excitation cascade. Statistical models and dynamical calculations have been used in an attempt to interpret the experimental data.

I. INTRODUCTION

Over the past few years, a systematic investigation of the properties of hot nuclei has been initiated.[1] Hot nuclei are now routinely produced in heavy-ion reactions. One of the important questions in studies of these nuclei is to establish whether the hot nuclei are significantly different from cold nuclei. For this purpose, one can get information on the excited nuclei by detecting the evaporated light particles and fragments. These emissions reflect the behavior of the nucleus at various stages of the de-excitation cascade.

For two different nuclei, estimates of some mean lifetimes for excitation energy equilibration (lower shaded band), collective deformation (upper shaded band), neutron emission (solid curves), and cumulative decay times for neutron emission (dashed lines) are shown in Fig. 1. These estimates have been done using the results from analytical estimates, empirical analyses, and Boltzmann-Uehling-Uhlenbeck (BUU) calculations.[2] In this paper we study the decay properties of a medium-mass nucleus ($A \sim 160$) at excitation energy near 300 MeV. For such high excitation energy, the time scale of the evaporation process approaches the time scale of energy equilibration and becomes shorter than that of nuclear deformation. One might thus expect an enhancement of nuclear dynamic effects and, therefore, a change of the physical ingredients in the statistical models which successfully describe the properties of nuclei at lower excitation energy.

Collective decay modes like the fission process provide a natural framework for the study of dynamical effects in the hot nucleus. The competition between evaporation and fission which is governed by statistical considerations at low temperature seems to be more sensitive to the nuclear dissipation at high temperature.[3] To study such effects, it is important to inquire first whether a statistical equilibration has been achieved in the hot nucleus. If this can be established, the statistical and dynamical proper-

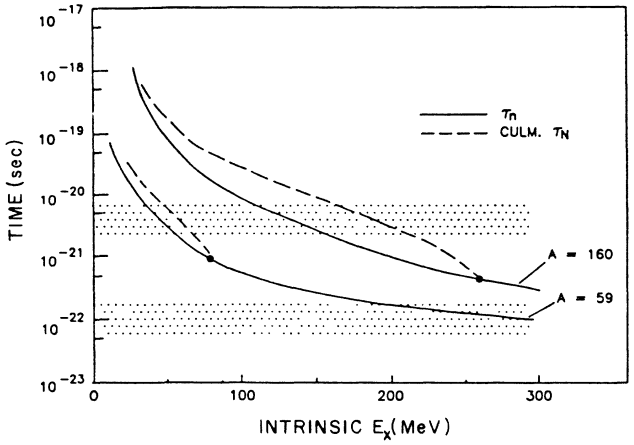

FIG. 1. Characteristic time scales for neutron emission, energy equilibration, and shape deformation (Ref. 2). (See text.)

ties of the system can be studied through determinations of multiplicities and energies of emitted species.

The organization of the paper is as follows: We shall describe in Sec. II the experimental procedures. Sections III and IV are devoted to the fusion-evaporation channel and the fissionlike channel, respectively. In each of these two sections, data and results from statistical and dynamical calculations are presented. In Sec. V, we compare the data of the fusion-evaporation channel with the data of the fissionlike channel. Remarks and conclusions are contained in Sec. VI.

II. EXPERIMENTAL PROCEDURES

To clarify the properties of hot nuclei with $A \simeq 160$, we have employed the ^{60}Ni+^{100}Mo reaction at 9.2 and 10.9 MeV/nucleon bombarding energy and detected both the light charged-particle emission and neutron emission in coincidence with evaporation residues and fission fragments. The reaction and bombarding energies were selected to produce nuclei with well-defined excitation energies near 300 MeV. The residue and fissionlike triggers were selected to isolate the most central collisions. Some results for the evaporation residue data were already published in letter form.[4]

The experiment was performed at the Argonne Atlas Accelerator Facility. A self-supporting ^{100}Mo target of thickness 420 μg/cm was bombarded with 550 and 655 MeV ^{60}Ni ions. The experimental arrangement is shown in Fig. 2. An electrostatic deflection system ($\pm$25 kV) was used to separate fusion residues from the beam. Si surface-barrier detectors divided into seven strips were used to detect the evaporation residues at various angles in a plane perpendicular to the light particle detector plane. The distance between these detectors and the target was 113.5 cm. A collimator ($\pm$1°) was set in front of the deflector plates to reduce elastic scattering and slit scattering into the evaporation residue detectors. Light charged particles were detected using three Si telescopes consisting of 50, 300, and 2000 μm backed by CsI crystals placed at θ=30°, 60°, and 75°, one telescope consisting of 20, 200, and 5000 μm placed at θ=90° and two telescopes consisting of 200 and 5000 μm placed at θ=135° and 150°. On the opposite side of the beam, four (5 in.×2 in.) liquid scintillator detectors made of NE 213 were used to detect neutrons at θ=45°, 90°, 110°, and 130°. Fission fragment energies and masses were obtained with two Si detectors (150 μm) set on each side of the beam ($\pm$18°).

The excellent time structure of the rebunched beam ($\simeq$500 ps) was used in the measurement of velocities of the residues, determinations of the masses of the light charged particles emitted at θ=135° and 150°, and determinations of the neutron energies. The telescope energy calibrations were done using ^{228}Th and ^{252}Cf sources and standard range energy curves. The "plasma" time delay in the Si detectors has been estimated using the results of Neidel *et al.*,[5] and the pulse-height defects have been corrected using the systematics of Ogihara *et al.*[6] The time of flight was used to separate neutrons from gamma rays (228.5 cm flight path). All neutron detectors were

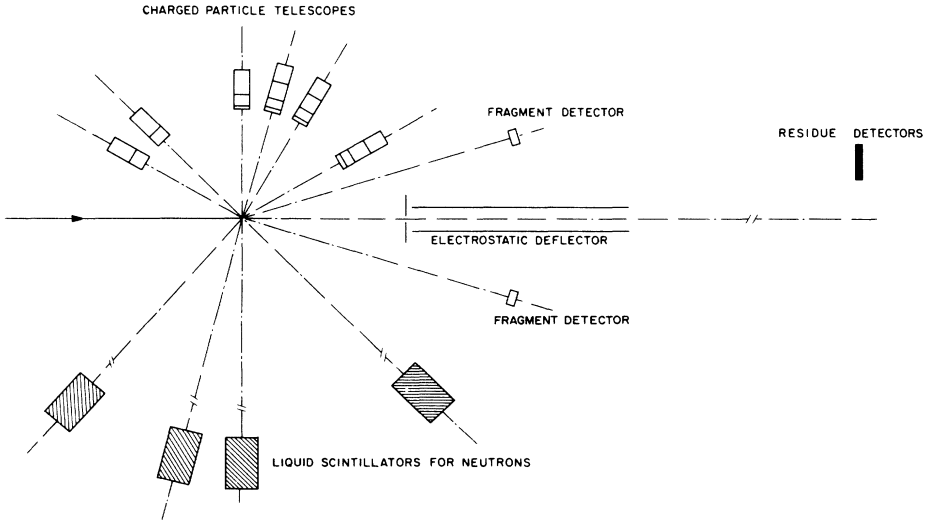

FIG. 2. Schematic of the experimental arrangement.

shadowed from the Faraday cup by thick concrete blocks and borated plastic sheets. In order to estimate the in-beam background, several runs were done with iron shadow bars set in front of each neutron detector. The neutron detector efficiencies were calculated using a Monte Carlo code of Anghinolfi *et al.*[7] and normalized to data obtained with a ^{252}Cf source.

III. FUSION EVAPORATION

A. Data and statistical model calculations

As can be seen from Fig. 3, the invariant velocity spectra of the evaporation residues show well-defined Gaussian distributions. The mean velocity observed in each detector strip is presented in Fig. 4. For each energy a dashed line indicates the velocity corresponding to a total linear momentum transfer. At 9.2 MeV/nucleon the mean velocity is that expected for complete fusion.[8] At the higher bombarding energy of 10.9 MeV/nucleon, the velocities of evaporation residues indicate an incomplete fusion characterized by about 94% linear momentum transfer from the projectile to the target. Using the massive transfer picture, the average kinetic energy carried away by the nonfused particles is about $\simeq 44$ MeV. From these results, we are able to derive the excitation energy of the emitted hot composite nucleus.

Since the residue velocity indicates that, for these central collisions, the threshold of an incomplete fusion mechanism is passed between 9.2 and 10.9 MeV/nucleon preequilibrium emission of light particles may be expected at the higher bombarding energy. This is confirmed in Fig. 5 where α-particle and proton spectra observed in coincidence with evaporation residues are shown at $\theta = 30°$, the most forward angle of observation for the light charged particles. The solid lines represent the thermalized moving-source parametrization for emission from the recoiling hot nucleus. The parameters have

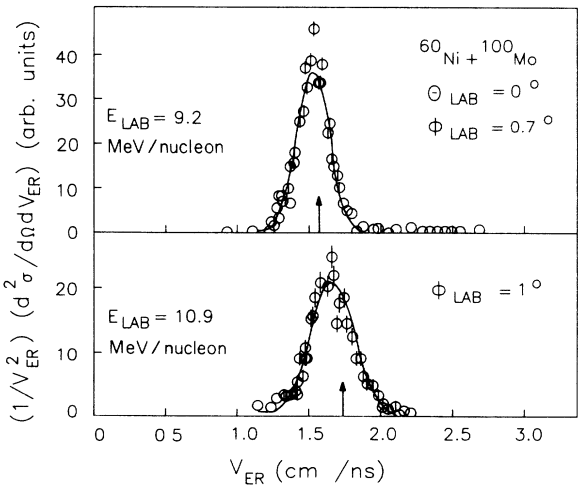

FIG. 3. Invariant velocity spectra for the evaporation residues at the two bombarding energies. The arrows show the velocities corresponding to complete fusion.

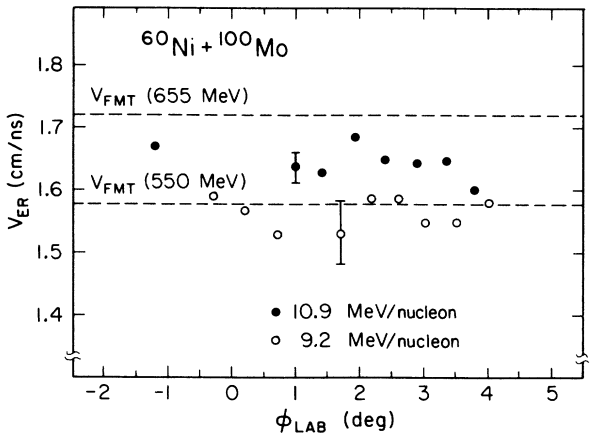

FIG. 4. Mean residue velocity observed in each detector strip at both bombarding energies. The lines indicate velocities for full linear momentum transfer.

been determined from a global fit to data at all detection angles. For both particle types, an additional high-energy component is observed only at 10.9 MeV/nucleon. This preequilibrium emission is not observed at larger angles where the light particle spectra in coincidence with evaporation residues exhibit one component representing the equilibrated statistical evaporation of the hot compound nucleus. Thus, for these central collisions leading to nonfissioning evaporation residues both the residue velocity measurements and the light particle spectra place the threshold of the incomplete fusion process near 10 MeV/nucleon. This value has previously been deduced from residue velocity measurements as a velocity threshold ($V_T = 1.8 \pm 0.6$ cm/ns) for the lighter reaction partner.[9] Above this threshold ($V_1 > V_T$), some nucleons escape the compound nucleus Fermi sphere before statistical equilibration.

To obtain good statistics for the coincidence runs, we have detected the evaporation residues at zero degrees. This has allowed an excellent isolation of the fusion-evaporation mechanism from other mechanisms as shown in Fig. 6 where the mass distributions of all species detected for the two excitation energies 293 and 251 MeV are presented. The evaporation residue peaks resulting from the central collisions are clearly shown. The elastic peak at $A = 60$ is sharply reduced. Taking into account the preequilibrium emission observed at the higher bombarding energy and using the average residue masses observed for the two excitation energies, we find the hot nucleus loses 16.4 ± 2 MeV of excitation energy per evaporated mass unit. This value is consistent with the value 14 MeV resulting from statistical model calculations (as discussed below) which include only n, p, α-particle, and gamma emission. While the detection of the residues at zero degrees discriminates against cases in which fragments are evaporated, the fragment evaporation is not expected to have an appreciable contribution to the de-excitation cascade at these excitation energies ($E_{\rm exc}/A \leq 2$ MeV).[10]

To deduce the parameters characterizing the de-

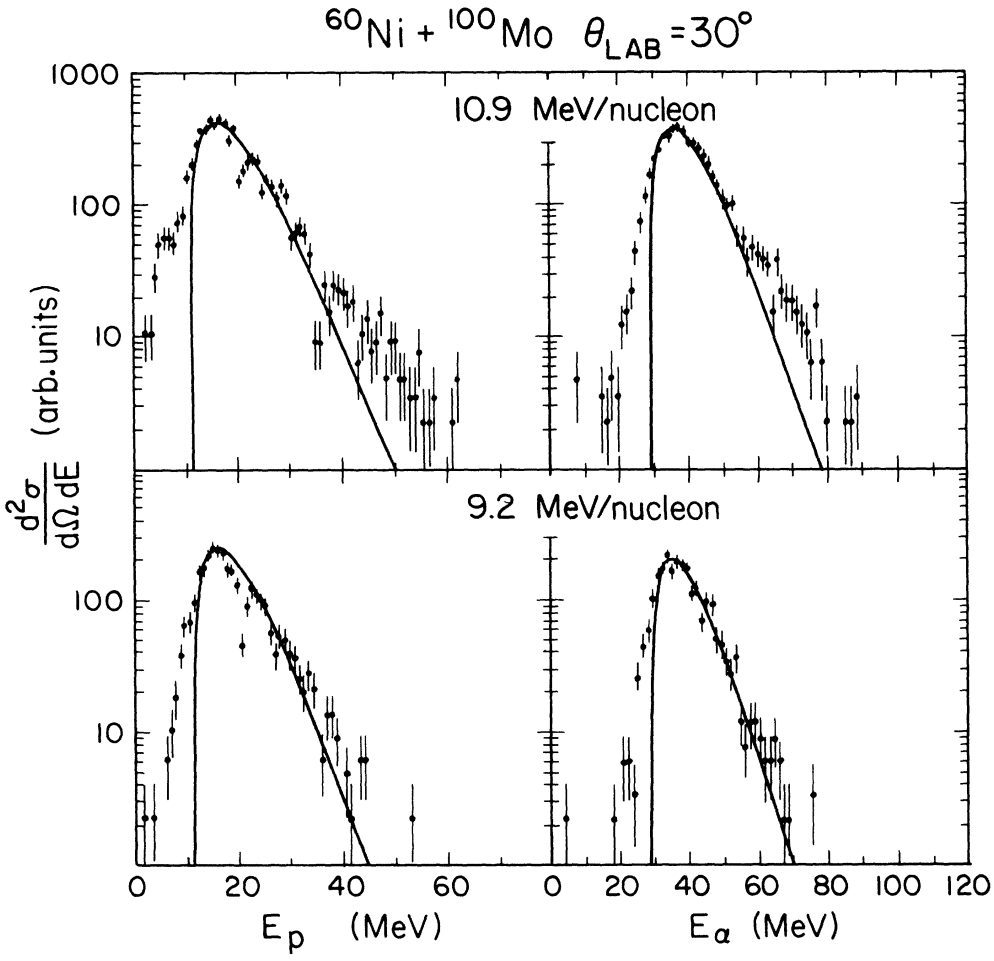

FIG. 5. Proton and α-particle spectra in coincidence with evaporation residues. The solid lines represent the thermalized moving source fit.

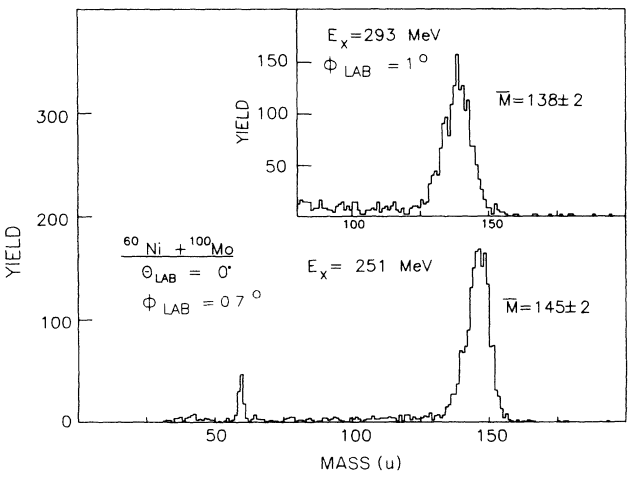

FIG. 6. Mass distributions corresponding to the two excitation energies. The mean values for the evaporation residue masses are indicated.

excitation cascade of the hot nucleus, i.e., the light evaporated particle multiplicities, the emission barriers, and the apparent and initial temperatures, we have fitted the evaporation spectra by surface Maxwellian-like distributions in the moving nucleus frame. The procedure followed to calculate these parameters for the neutron, proton, deuteron, triton, and α-particle emission was previously published.[4] The light charged-particle spectra have been fitted by a surface Maxwellian function $(E-B_c)\exp[-(E-B_c)/T_{app}]$ and the neutron spectra have been fitted using the expression $E^{1/2}\exp(-3E/4T_{app})$. The parameters E, B_c, and T_{app} represent, respectively, the channel decay energy, the emission barrier, and the apparent temperature. The difference spectra, obtained by subtracting the spectra observed at 550 MeV bombarding energy from those at 655 MeV, have been fitted by surface Maxwellian functions to determine the average parameters corresponding to the "quasi-first-chance" emission spectra. We refer to those temperatures as initial temperatures. For neutrons and tritons, we also have determined the initial temperatures by us-

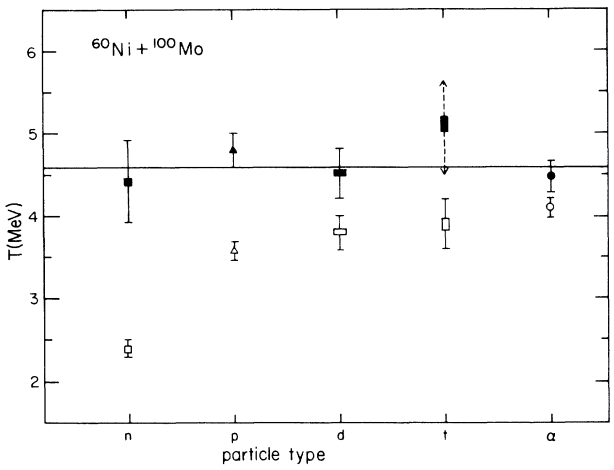

FIG. 7. Apparent (open dots) and initial (solid dots) temperatures for the particle evaporation at 293 MeV excitation energy. The solid line at $T=4.62$ MeV shows the average initial temperature.

ing, for the average energy of the difference spectrum, the expression[11]

$$\langle E_{\text{init}} \rangle = \frac{M_2\langle E_2 \rangle - M_1\langle E_1 \rangle}{M_2 - M_1} = 2T_{\text{init}} ,$$

where M represents the multiplicities and where the subscripts 1 and 2 refer to the low and high excitation energies. The results are presented in Fig. 7 and in Table I. Neutron emission is the dominant decay mode of hot medium-mass nuclei, reflecting Coulomb barrier effects for the charged-particle emission. At the higher excitation energy of 293 MeV, the emission of 14.8 neutrons takes away about 219 MeV excitation energy from the hot nucleus. This value has been estimated using the average kinetic energy, the multiplicity, and an average Q value for the neutron emission.

Light charged particles are emitted preferentially in the early steps of the de-excitation cascade. Evidence for this is seen in Fig. 7, where the initial temperature of the hot nucleus at 293 MeV excitation energy is compared with the apparent temperatures representing the entire de-excitation cascade. The increase of the apparent temperature with the type of the emitted particle suggests a more favorable emission probability at the higher excitation energies for the charged particle. Even though the decay probability is less favorable for the neutrons at the higher excitation energies, we derive, within experimental error, the same initial temperatures for all daughter nuclei produced in first-chance emission (all these daughter nuclei are produced at approximately the same excitation energy). This provides strong evidence of thermal equilibrium in the primary nucleus.

When the nucleus is heated to 300 MeV excitation energy, an evolution of the nuclear properties is observed. Assuming the validity of the degenerate Fermi-gas model, the apparent increase of the density of states with the excitation energy is less than one could have expected based on low-energy data. We have obtained a value for the level density parameter a of 11.1 ± 0.6 MeV^{-1} ($A/a=13.8\pm0.7$ MeV) for the daughter nucleus at 236 MeV thermal excitation energy (see Ref. 4). At low excitation energy, this parameter is 19 ± 1.5 MeV^{-1}.[12] The decrease of a was already observed in the α-particle de-excitation channel in previous experiments.[13,14] This strong variation of the level density parameter can be reproduced by several theoretical calculations.[15–17] These works have shown that the temperature variation of the frequency-dependent effective mass of the nucleon reduces the parameter a at high excitation energies, but a complete description of the temperature dependence of the level density is still needed.

The emission barrier extracted from the evaporation spectra using the simple parametrization $(E-B_c)\exp[-(E-B_c)/T]$ changes with the temperature of the hot nucleus. At 293 MeV excitation energy and for the integrated α-particle emission spectra (plotted in Fig. 8), we observe effective emission barriers of 11 MeV for the "quasi-first-chance" emission spectrum (middle spectrum) and 13 MeV for the total de-excitation cascade emission spectrum (bottom spectrum). At 251 MeV excitation energy (top spectrum), the average emis-

TABLE I. Apparent temperatures, multiplicities and emission Coulomb barriers for light particles emitted by the hot nuclei.

E_x (MeV)	Particle	T_{app} (MeV)	$\overline{M}$	B_c (MeV)
293	α	4.07±0.10[a]	0.901±0.200	13.0±0.5
	t	3.90±0.30	0.073±0.010	8.0±1.0
	d	3.82±0.20	0.190±0.020	6.2±1.0
	p	3.58±0.10	1.32±0.20	5.5±0.8
	n	2.401±0.100	14.80±0.50	
251	α	3.78±0.10[a]	0.579±0.150	14.0±0.5
	t	3.59±0.30	0.058±0.010	8.0±1.0
	d	3.48±0.20	0.131±0.020	6.0±1.0
	p	3.27±0.10	1.10±0.15	6.5±0.8
	n	2.240±0.100	13.74±0.50	

[a]Angular momentum corrected values (see Ref. 4).

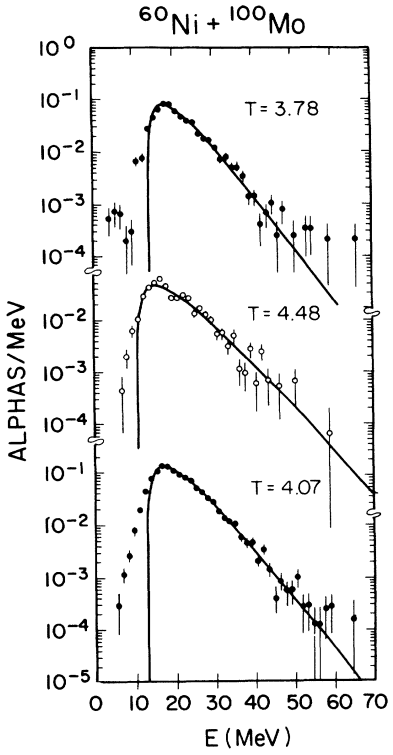

FIG. 8. Energy spectra of α particles at 251 MeV excitation energy (top spectrum) and 293 MeV (bottom spectrum) in the moving-source frame. The middle spectrum is obtained by subtracting the top spectrum from the bottom spectrum. The lines show the single-source fits.

sion barrier is 14 MeV. Similar trends have been observed for the proton emission. A systematic reduction of the emission barriers at high excitation energies has been observed by Parker *et al.*[18] Such a reduction might be due to an increase of static deformations, shape oscillations, or modified density distributions of the hot nucleus.[19]

The parameters characterizing the hot nucleus can be compared with statistical model estimates. For this purpose we have used the code CASCADE.[20] At 251 MeV excitation energy and for an average inverse level density parameter ($K = A/a$) $K = 10$ MeV, the predictions for the evaporation multiplicities are 8.17 neutrons, 3.12 protons, and 1.73 α particles. These calculations overestimate the light charged-particle emission and underestimate the neutron emission (see Table I). We note, however, that the calculation predicts an evaporation of 18.2 evaporated mass units which is reasonably consistent with the experimental mass of the evaporation residue 145±2 found at 251 MeV excitation energy (see Fig. 6).

A formal way to reproduce the experimental multiplicities is to cut artificially the charged-particle de-excitation cascade below some excitation energy.[21] For example, with a threshold of 120 MeV for light charged-particle emission and using an average inverse level density parameter of $K = 11$ MeV, reflecting the higher average excitation energy for the charged-particle emission, the calculated multiplicities are 0.75 proton and 0.65 α particle. The discrepancy between the calculated and the experimental proton multiplicities indicates a lower emission threshold for the protons than for the α particles. Surely these artificial thresholds are too high and must be taken only as an approximation of a smoother emission probability distribution. On the other hand, this result is qualitatively consistent with our previous work[22] for the $^{14}N + ^{154}Sm$ reaction. In that reaction we observed a low probability of α-particle emission in coincidence with evaporation residues below $\simeq 100$ MeV thermal excitation energy. It appears that statistical models like CASCADE do indeed overestimate the emission of light charged particle below $\simeq 100$ MeV for medium-mass nuclei.[20] This effect might originate from angular momentum effects which are not handled correctly in these statistical model calculations. We performed different statistical model calculations to check the results obtained with CASCADE. Using the code PACE2 (Ref. 23) at 251 MeV, for instance, we found 7.01 neutrons, 3.06 protons, and 2.41 α particles, which are close to the CASCADE predictions.

As previously pointed out, the apparent temperature should reflect the dependence of the emission probability with the excitation energy. Using the sharp threshold for the onset of charged-particle emission and assuming $a = A/11$ at an excitation energy of 251 MeV, we find a calculated apparent temperature of 3.66 MeV which is close to the experimental value. We can go a step further by summing this calculated spectrum with a spectrum calculated starting at 293 MeV but allowing only two decay steps (with $a = A/13.8$ MeV^{-1}). The resultant spectrum may be compared to the total de-excitation spectrum at an initial excitation energy of 293 MeV excitation energy. The fit gives an average temperature of 4.06 MeV almost equal to the experimental one. This simulation with the statistical model provides some confidence in the subtraction technique used to obtain the "quasi-first-chance" emission spectra[4] which assumes negligible differences in the de-excitation cascade for the nuclei produced at 293 MeV excitation energy and those produced at 251 MeV excitation energy.

For the α-particle emission in the nuclei considered here the potential barrier extracted from optical-model parametrizations is about 18 MeV. This value is significantly higher than the experimental value. Similar behavior has been observed many times and interpreted in terms of static nuclear deformation or a modified density distribution. In some studies, the static deformation has been simulated in the calculations by increasing the radius of the spherical nucleus thus modifying the optical-model transmission coefficients.[24] We have applied this technique in an attempt to reproduce the "quasi-first-chance" emission spectra at 293 MeV excitation energy. The transmission coefficients have been generated using optical-model parameters from Huizenga and Igo.[25] In order to evaluate deformation effects, the "quasi-first-chance" spectrum provides a better basis than the spectra resulting from the whole de-excitation cascade since the complexity of the total decay cascade requires one to deal with average values which are less meaningful. In Fig. 9, both the experimental and calcu-

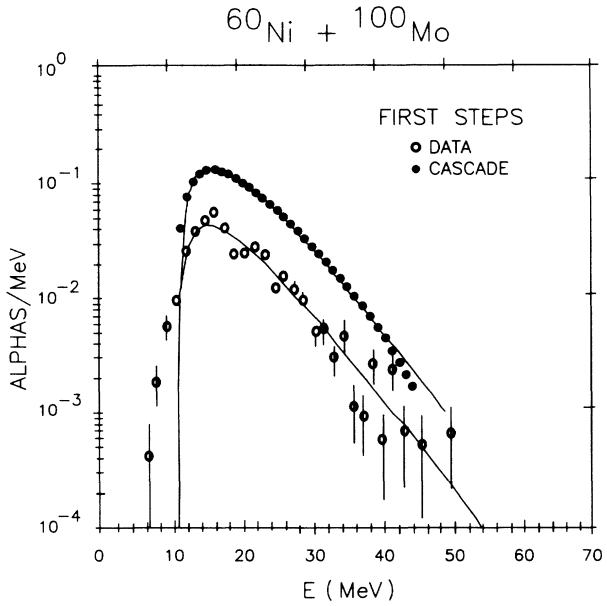

FIG. 9. Statistical model prediction (solid points) and experimental data (open circles) for the α-particle "quasi-first-chance" emission spectrum at 293 MeV excitation energy in the moving-source frame. Solid lines represent a surface evaporation emission $(E-B_c)\exp[-(E-B_c)/T]$. See text.

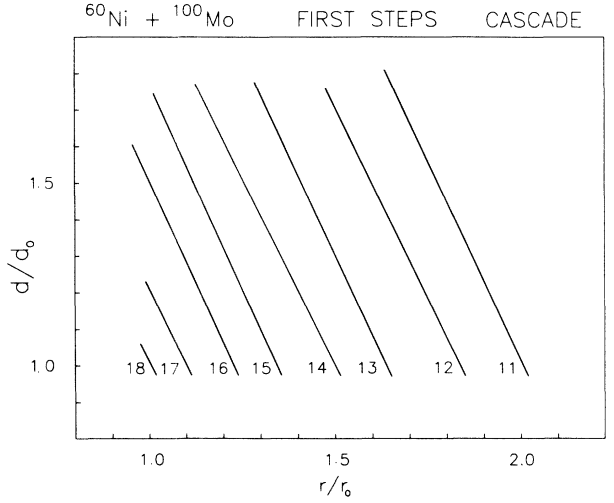

FIG. 10. Correlation in the optical-model calculation between the diffuseness (d) and the radius (r) for different emission barriers. d_0 and r_0 refer to the standard parameters (Ref. 25).

lated α-particle spectra are shown. The slope of the spectrum from the two first decay steps ($a = A/13.8$ MeV^{-1}) reproduces the experimental initial temperature. The observed Coulomb barrier for the emission (11 ± 0.5 MeV) requires an increase by a factor of two in the optical-model radius. For the proton emission the reduced emission barrier (4.5 ± 1.0 MeV) also requires important modifications for the optical-model parameters. The change of the optical-model radius required by the "quasi-first-chance" α-particle spectra can be slightly attenuated by increasing the value of the diffuseness parameter. The correlations between these two parameters from $B_c = 11$ MeV to $B_c = 18$ MeV are shown in Fig. 10. A variation in the diffuseness parameter represents a change in the density distribution at the surface of the hot nucleus. Assuming volume conservation, a value of $r/r_0 = 1.5$ corresponds to axis ratios of 3.37/1 and 1.83/1 for oblate and prolate shapes, respectively, and a value of $r/r_0 = 2.0$ leads to axis ratios of 8/1 and 2.82/1, respectively. Because the statistical model normally assumes spherical nuclei, the calculations with these reduced barriers lead, as is apparent in Fig. 9, to an overprediction of the α-particle multiplicity for the "quasi-first-chance" emission.

The axis ratios suggest that the elongation of the hot nucleus could be significant for static deformations. For nuclei $A \simeq 160$ with an average angular momentum $l \simeq 45\hbar$, the rotating cold liquid-drop model[26] has predicted a slight oblate deformation $b/a \simeq 1.2/1$ for the ground-state configuration. This elongation could not explain the emission barrier for the "quasi-first-chance" emission spectra.

In an attempt to explain the α-particle emission barrier, we might consider the possibility of "superdeformed" oblate shapes for the rare-earth nuclei since some calculations[27] have predicted a 2 to 1 major to minor axis ratio at high spin which is correlated with the existence of fission isomers. Nevertheless, the shell effects which give rise to these "superdeformed" shapes should disappear for temperatures higher than 3 MeV (Ref. 28) and, in addition, these "superdeformed" states take place only for the highest angular momenta while the "quasi-first-chance" emission spectra do not restrict the spin of the emitting nucleus to these high values. Thus, the strong reduction of the emission barrier in the "quasi-first-chance" emission more likely originates from dynamical deformations. It should be pointed out that the "quasi-first-chance" emission spectra include only equilibrium emission. The preequilibrium contribution has been excluded (see Ref. 4).

B. Emission barriers and dynamical calculations

In order to see whether dynamical effects could play a role in the "quasi-first-chance" emission spectra, the transport equation of Vlasov-Uehling-Uhlenbeck (VUU) has been solved for the ^{60}Ni+^{100}Mo reaction (10.9 MeV/nucleon bombarding energy) in a central collision ($b = 0$ fm). The dynamics of the collision is predetermined by the time dependent mean field in the Vlasov term and by the in-medium nucleon-nucleon cross section in the collision term. The calculations are fully presented in Ref. 29. A reduced numerical uncertainty of the total energy allows us to use this model at low bombarding energies. The time evolution of the density distribution is described in Fig. 11 up to 500 fm/c (1.65×10^{-21} s). As can be seen, the damping of the initial collective energy along the beam axis (z axis) results in rather important deformations. Part of the initial energy leads to

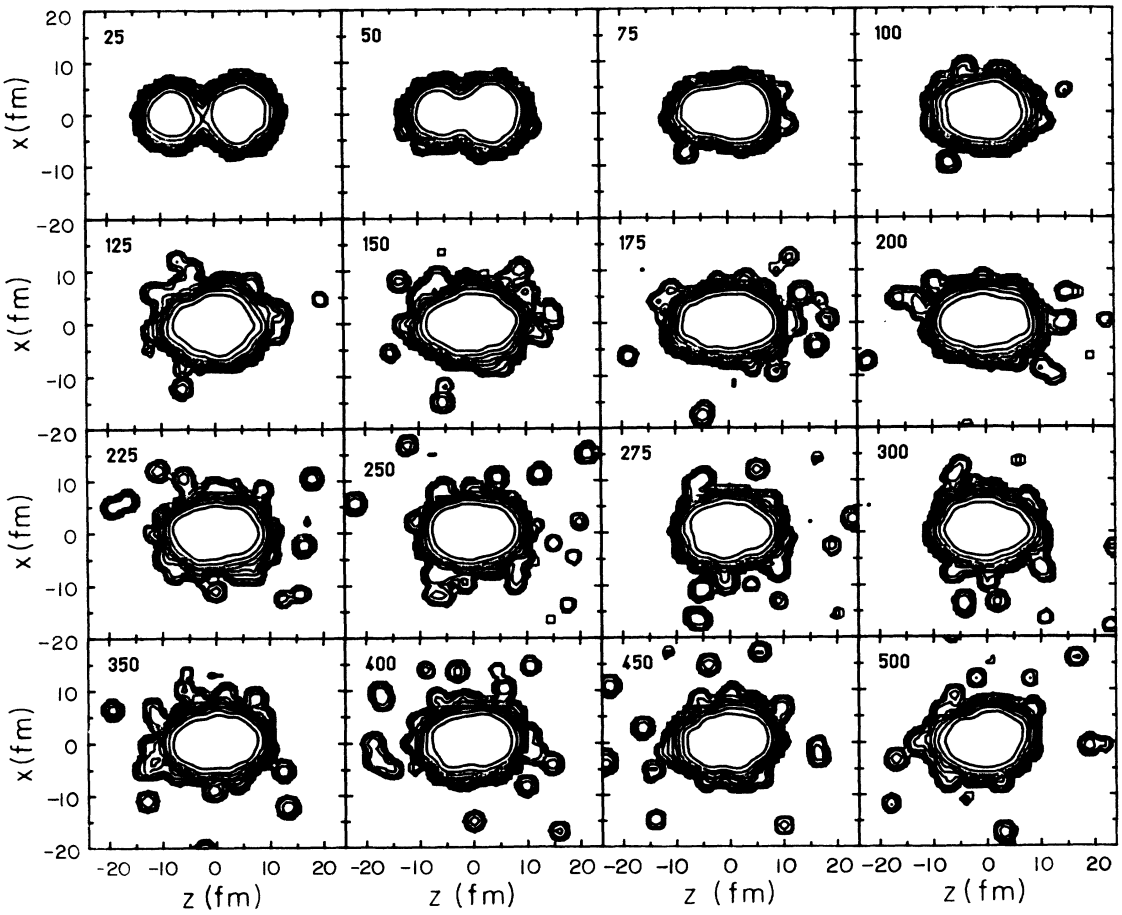

FIG. 11. Time evolution of the density distribution $\rho(z,x,y=0,t)$ for a central collision of $^{60}Ni+^{100}Mo$ at 10.9 MeV/nucleon. The time is given in units of fm/c.

compression-extension modes (monopole, quadrupole, etc.). The amplitudes of these collective motions can be seen in Fig. 12(a) where the time evolution of the radii along the z axis and x axis are presented. We note that the relaxation of the collective motions takes a rather long time. Figure 12(b) shows the evolution of the collective kinetic energy $E_{\rm coll}$ (which includes the kinetic energy carried away by the emitted particles) as well as the evolution of the intrinsic excitation energy E^*.

Let us now follow the time evolution of the collision. The maximum overlap between the projectile and the target occurs at $\simeq 100$ fm/c ($\simeq 3\times 10^{-22}$ s) which corresponds to a maximum intrinsic excitation energy and therefore a minimum collective kinetic energy. At that time, according to the calculations, light particle emission starts. The energy per unit of time carried away by these particles peaks near 150 fm/c (the delay represents approximately the time needed to escape the system) as can be seen from Fig. 13. This emission during the first step of the collision should correspond to a preequilibrium emission. The integrated energy taken away by this peak reaches 60 MeV (Fig. 13) which is comparable to the preequilibrium energy estimated from the evaporated residue data (44 MeV). After $t\simeq 150$ fm/c, evaporation emission takes place, cooling down the hot nucleus. At this stage, however, the hot nucleus still evolves with different relaxation times for the collective degrees of freedom and the emission of light particles. At 175 fm/c, the total collective energy is about 150 MeV (± 50 MeV) which corresponds to a value of $\simeq 80$ MeV for the kinetic energy of the collective oscillations. We note that at 175 fm/c the preequilibrium emission phase is ended. Since this time is in reasonable agreement with the estimated particle evaporation lifetimes shown in Fig. 1, we focus on 175 fm/c as a time to estimate the effects of the collective motion on the particle emission. The hot nucleus is now strongly deformed in the z-axis direction, with a 1.6/1 axis ratio.

Using the density distribution of the hot nucleus calculated with the VUU equation and following the optical-model procedure, an estimation of the emission barriers for an α particle has been done at 175 fm/c. Figure 14 shows the nuclear potential resulting along the z axis and x axis, respectively, and the corresponding values for the transmission coefficients. The VUU potential has been fitted with a standard Woods-Saxon (WS) potential used in statistical model calculations. Some discrepancies appear at the surface of the hot nucleus resulting from statistical fluctuations in the test-particle method used in the calculations. Based on the VUU density distribution, the

value of the emission barriers are 11.8 MeV along the z axis and 18.5 MeV along the x axis. The higher emission barriers obtained with the WS potential, 13.5 and 18.0 MeV, respectively, emphasize the role of the density distribution at the surface of the deformed nucleus. We note that the emission barriers along the z axis deduced from the VUU calculations are consistent with our experimental value deduced from the "quasi-first-chance" emission spectra (11.0±0.5 MeV). Nevertheless, whether α particles could be emitted predominantly from the surface where the emission barrier is the lowest is an open question. One might expect a weighted average emission barrier for the deformed nucleus between 11.8 and 18.5 MeV. In such a case, our lower experimental emission barrier could indicate that the calculations have underestimated the amplitude of the collective motion.

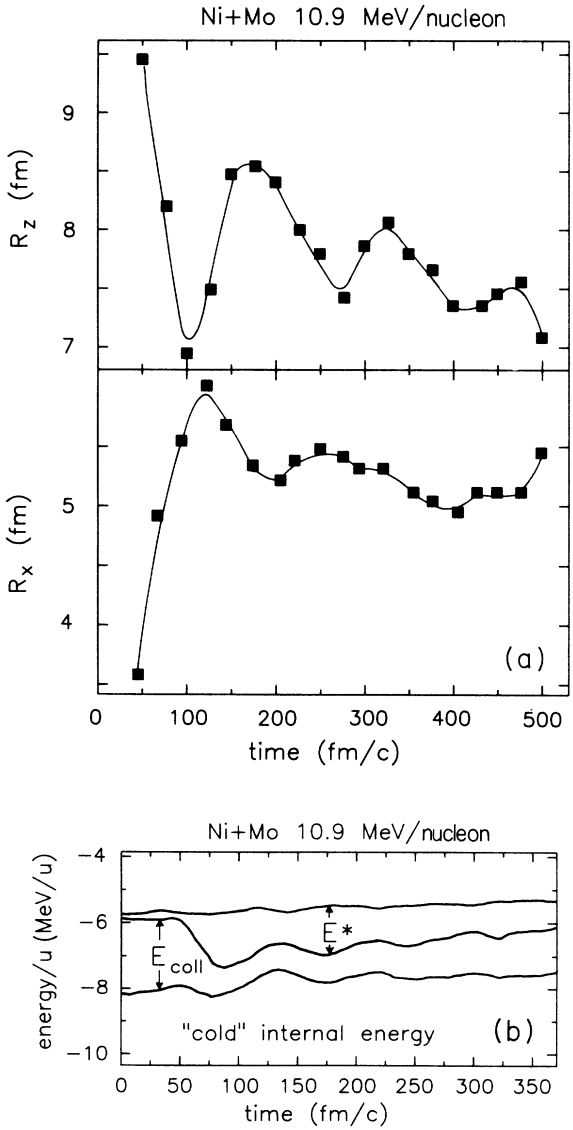

FIG. 12. (a) Time evolution of the radii along the z axis and x axis. See text. (b) Time evolution of the total energy for the system. See text.

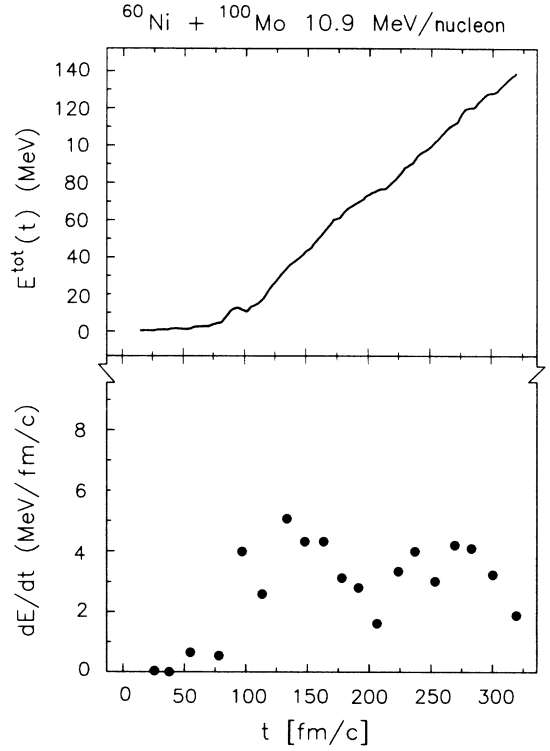

FIG. 13. Differential and integrated kinetic energy of the emitted particles versus the time according to the VUU calculation for ^{60}Ni+^{100}Mo at 10.9 MeV/nucleon.

The magnitude of these oscillations is determined mainly by the incompressibility modulus associated with the effective interaction.

Because of the statistical fluctuations included in the VUU calculations, a different approach could be used to estimate the emission barrier for the α particle at 175 fm/c. This approach consists of taking the VUU calculations to get the deformation of the hot nucleus and of using the Hartree-Fock description to calculate its diffuseness. This model predicts a small thermal expansion of the nuclear matter at high temperatures due to variations of the density distribution at the surface. Using the Skyrme effective interaction SIII, Saurer *et al.*[30] have deduced that the density diffuseness increases with the temperature T as $d(T)=d_0(1+9\times10^{-3}T^2)$. By assuming that the increase of the rms radii with the temperature is mainly due to this variation in the diffuseness, we reproduced the results of Bonche *et al.*[31] for the SIII effective interaction. With the SKM effective interaction associated with a stronger variation of the radii with the temperature, we deduced the following expression for the temperature dependence of the diffuseness:

$$d(T)=d_0(1+14\times10^{-3}T^2)\ .$$

A similar variation for the diffuseness in the nuclear potential has been considered. For temperatures near 5 MeV, the diffuseness could increase by a factor of 1.35. Thus an average deformation of $r/r_0=1.5$ along the beam axis due to compression-extension modes and a

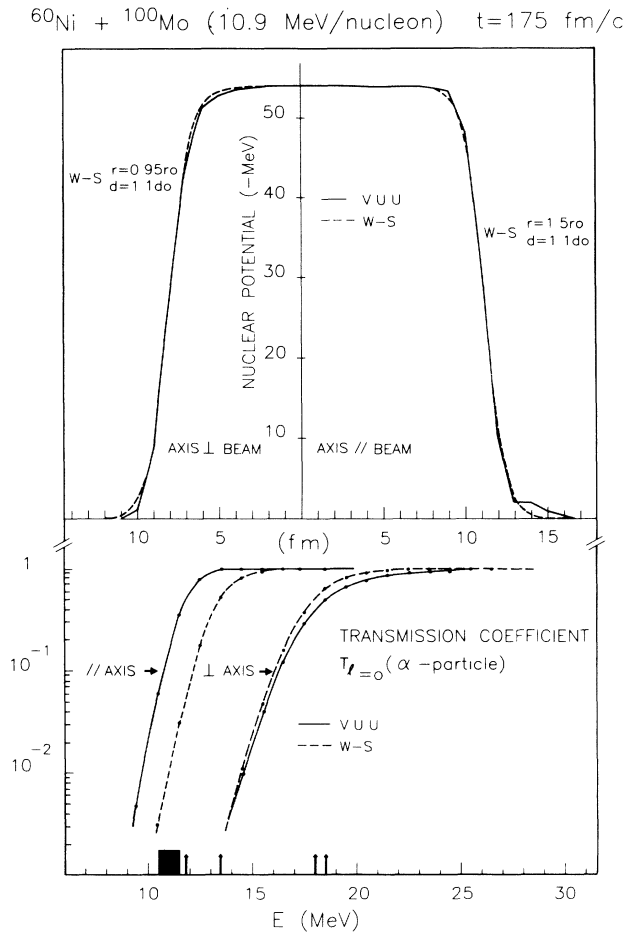

FIG. 14. Nuclear potentials and transmission coefficients for the α particle emitted along the $\parallel$ and $\perp$ axes at $t=175$ fm/c. See text.

diffuseness parameter of $d/d_0=1.35$ due to thermal expansion would lead, for instance, to an emission barrier of $\simeq 12.8$ MeV (Fig. 10), which can be compared with our experimental emission barrier of 11 MeV.

In addition to the effect on the emission barrier, the compression-extension modes will affect the extracted value of the level density parameter a for the hot nucleus. Correcting our excitation energies by subtracting the calculated collective kinetic energy at 175 fm/c, the apparent level density parameter could drop from $A/13.8$ to approximately $A/20$. This last value, which is low with respect to theoretical predictions,[32] might suggest that the calculation overestimates the collective energy or that the energy of the collective oscillations induces an energy enhancement in the spectra of the emitted particles.

We conclude from these calculations that the damping of the collective motions can modify the shape of the hot nucleus for a rather long time with respect to the lifetime of the hot nucleus. Compression-extension modes could reduce significantly the emission barriers for the charged particles.

IV. FISSIONLIKE EVENTS

A. Data and statistical model predictions

In order to investigate the emission of light particles in the fissionlike channel, we detected fragments at laboratory angles of $\pm 18°$. In Fig. 15 we show the fragment energy distribution at the lower bombarding energy. One can see fragments corresponding to quasielastic, deeply inelastic, and fissionlike reactions. Symmetric fission was selected by setting an energy bin indicated by the dashed lines. The observed energy is consistent with that expected from systematics.[33]

A comparison of particle spectra detected in coincidence with fission fragments detected on each side of the beam allows separation of the components of the light particle emission originating from pre-scission and post-scission emission. For example, the spectra of α particles in coincidence with symmetric fission fragments are shown in Figs. 16 and 17 for the two excitation energies. The laboratory angles and the triggers are indicated in the figures. The Maxwellian-like surface emission fits $(E-B_c)\exp[-(E-B_c)/T_{\rm app}]$ used to extract the temperatures, multiplicities, and emission Coulomb barriers are superimposed on the histograms. The dotted and dashed lines represent the contributions from the composite nucleus emission (pre-scission) and fully accelerated fragment emission (post-scission), respectively. The solid lines show the sum spectra of the particles from three emission sources. The velocity of the composite nucleus source has been taken from the evaporation residue results. The direction and velocity of the undetected fragment source have been determined from two-body kinematics and total kinetic energy systematics. Each fit has a single normalization for all the data. For the α-particle emission, we took recoil effects into account. The spectra of protons triggered by the fission detector set at $\theta=-18°$ are shown in Fig. 18 for the two excita-

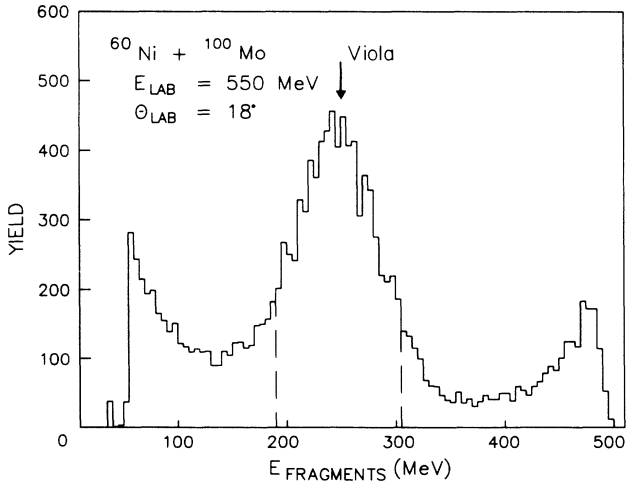

FIG. 15. Energy spectrum for heavy fragments detected at $\theta=18°$ for the lower bombarding energy. The dashed lines indicate the symmetric fission contribution.

tion energies. In the deuteron and triton cases, the statistics were too poor to extract meaningful fits.

Some deviations between the experimental light particle spectra and those obtained with the three-moving-source simulation have been observed at the most forward angle ($\theta=30°$) at both bombarding energies. A surplus of high-energy particles, present in the α particle and proton spectra, is ascribed to a nonequilibrium emission already observed in the evaporation residue channel. A more important surplus at low energy, observed only in the α-particle spectra and for the trigger set at $\theta=-18°$, is attributed to a near-scission emission. As can be seen in Fig. 19, the two different kinematics ($\pm 18°$) indicate clearly that this α-particle surplus originates from the neck region between the two fragments emitted predominantly perpendicular to the scission axis. This emission near the instant of scission is well known for low- and high-energy fission[34–36] and can result from a ternary fission process[37] or evaporation from the partially accelerated fragments just after scission. We observe a mean energy in the center of mass of about 8.5 MeV for this emission, consistent with the Coulomb

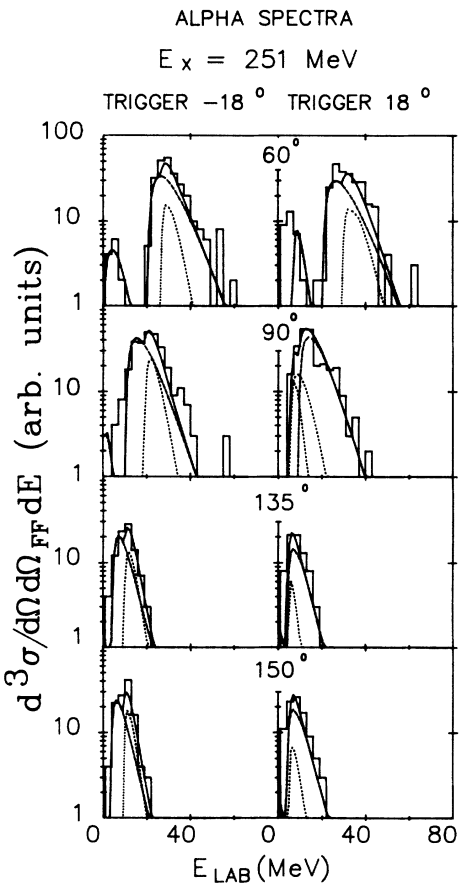

FIG. 16. Coincident α-particle spectra at 251 MeV excitation energy for different laboratory detection angles. The fragment trigger angles are indicated. Lines represent moving-source fits. The solid curves correspond to the sum of the composite nucleus emission (dashed line) and the fragment emission (dotted line).

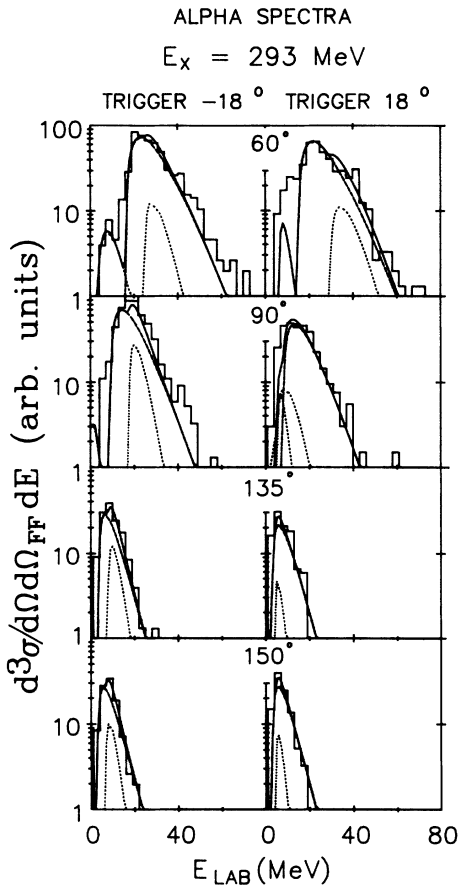

FIG. 17. Same as Fig. 16 but at 293 MeV excitation energy.

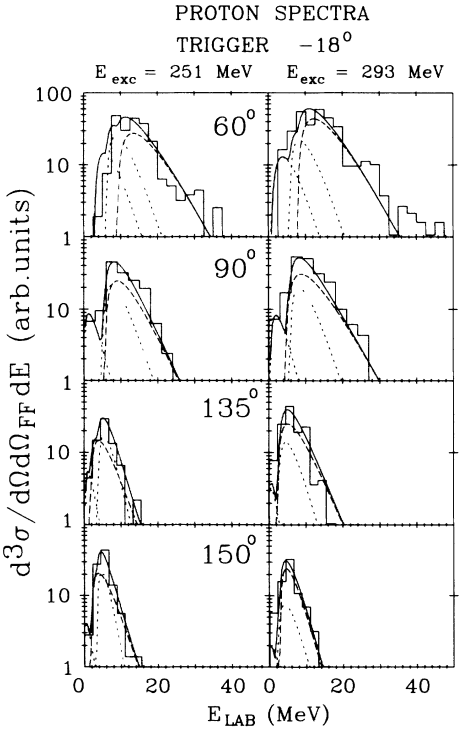

FIG. 18. Coincident proton spectra for the two excitation energies for one fragment trigger angle. Same notation as in Fig. 16.

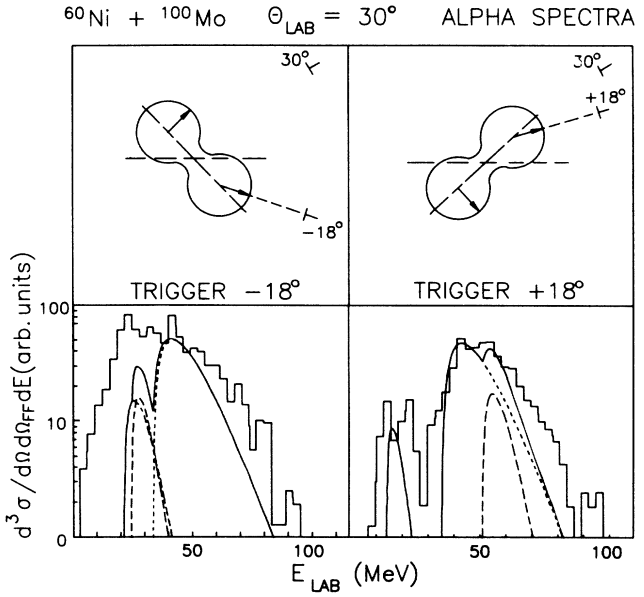

FIG. 19. Spectra of α particles detected at $\theta=30°$ for the higher bombarding energy. Same notation as in Fig. 16.

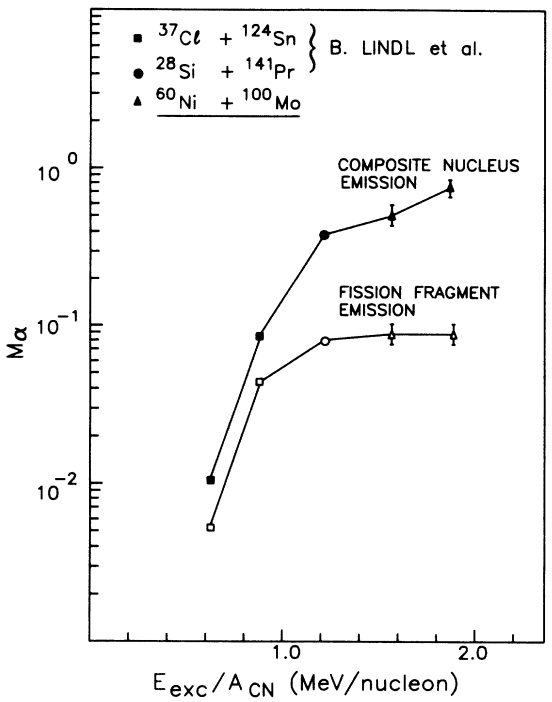

FIG. 20. Multiplicities of α particles for pre-scission and post-scission emission as a function of the excitation energy per nucleon in the compound nucleus. The present data are compared with data for lower bombarding energies (Ref. 36).

focusing from the adjacent fragments assuming low initial kinetic energy for an emitted α particle.[38] It should be emphasized that our pre-scission source includes presaddle and saddle-to-scission emission[39] but that the observed near-scission emission may occur during the descent from the saddle-to-scission point. Near-scission emission for protons has not been observed in the spectra. This may result from lower emission Coulomb barriers which reduce the anisotropy of the emission and the energy of the emitted protons.

We have determined pre-scission and post-scission multiplicities for the light particle emission assuming an isotropic out-of-plane distribution. Thus these calculations represent upper limits for the α-particle multiplicities. These are shown in Fig. 20, plotted versus the excitation energy per nucleon in the hot nucleus. Our data are compared with those obtained by Lindl *et al.*[36] for slightly different reactions and at lower bombarding energies. For the three reactions, the fission proceeds with comparable fission barrier heights.

At low excitation energy, the pre-scission and post-scission multiplicities follow the same trend, increasing with the excitation energy of the nucleus. Above approximately 1 MeV/nucleon excitation energy, the post-scission multiplicity remains constant. The increased excitation energy is taken away before the composite nucleus reaches the scission point. As a result, the fission process remains a relatively cold process. Recent studies of Hilscher *et al.*[40] show also this result in neutron emission measurements.

Some neutron spectra measured at $\theta=45°$ in coincidence with the fission fragments are shown in Fig. 21. The identification of the pre-scission and the post-scission emission has been done as in the charged-particle cases using the two triggers set on each side of the beam. Since the neutron multiplicities are large, implying a relatively

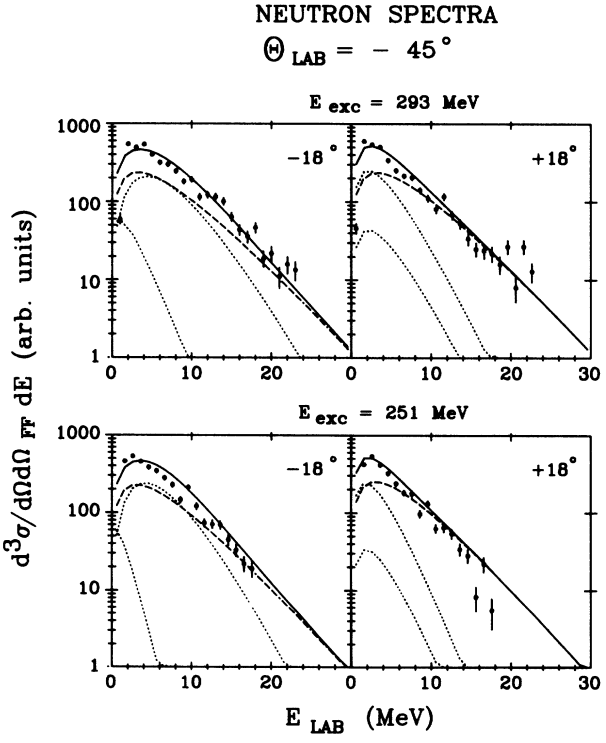

FIG. 21. Neutron laboratory spectra ($\theta=45°$) in coincidence with fission fragments detected at $\theta=\pm18°$ for the two bombarding energies. Same notation as in Fig. 16.

long emission cascade, we have used the function $E^{1/2}\exp(-3E/4T_{app})$ to fit the neutron data. The same formulation was previously used in the evaporation residue channel.[4] Because of the suppression of the Coulomb field, it was not possible to distinguish the near-scission emission. Further, since the neutron spectra do not contain Coulomb barrier effects, the relative contribution of the pre-scission and post-scission has been obtained with slightly larger uncertainties than in the charged-particle cases.

At 550 MeV bombarding energy, we have found post-scission multiplicities per fission fragment of $M_n=1.8(\pm0.5)$, $M_p=0.21(\pm0.05)$, and $M_\alpha=0.081(\pm0.02)$ for neutron, proton, and α-particle emission, respectively. At 655 MeV bombarding energy, the measured post-scission multiplicities are $M_n=2.3(\pm0.5)$, $M_p=0.22(\pm0.05)$, and $M_\alpha=0.080(\pm0.02)$. Although for neutrons, the error bars are larger, the multiplicities all show, within experimental error, a saturation with bombarding energy. The comparison of these values to calculated ones provides information about the excitation energy of the fission fragments. Using CASCADE and taking the primary fragment to be a nucleus with $A=75$ at 45 MeV excitation energy and $l\simeq10\hbar$, we find calculated multiplicities of 2.0, 0.28, and 0.075 for the neutron, proton, and α-particle multiplicities. These reproduce the magnitude of the relative multiplicities between the different particle emissions. We conclude that at each excitation energy, the fission fragments share about $\simeq90$ MeV of excitation energy.

The pre-scission multiplicities measured at the two bombarding energies are listed in Table II. The consistency of these results can be checked by calculating the energy balance in the fission process. At 251 MeV excitation energy, for example, from the apparent temperatures, emission barriers, and the multiplicities and calculating the Q values assuming a sequential emission of α particles, protons, and neutrons, respectively, it turns out that the pre-scission emission cools the hot nucleus down to $\simeq140$ MeV. We have deduced $\simeq90$ MeV for the total excitation energy of the fragments. The missing energy corresponds to the difference between the fission Q value and the fragment total kinetic energy (TKE) ($Q-\mathrm{TKE}\simeq-30$ MeV) and energy not accounted for by particle emission.

Comparisons of the experimental multiplicities with the statistical codes PACE (Ref. 23) and CASCADE have been done. The fission barrier heights were calculated using the Yukawa-plus-exponential finite-range model.[41] Based on the energy balance of the fission process, the CASCADE calculations have been made using a cutoff at 140 MeV excitation energy. The experimental and calculated multiplicities are contained in Table II. One of the important features as previously observed[42,43] is that none of PACE2 and CASCADE predictions can reproduce the large number of neutrons, protons, and α particles emitted before scission providing strong evidence for dynamical effects in the fission process.

Our total multiplicities for neutrons and α particles are shown together with other data for medium-mass nuclei in Fig. 22. We observe a change of the rate of increase of the neutron multiplicity with excitation energy which corresponds to the start of α-particle emission. The α-particle emission is small below 100 MeV because of the emission Coulomb barriers. The same threshold was deduced for the evaporation residue channel using statistical calculations.

B. Pre-scission multiplicities and dynamical calculations

Over the past decade, several groups[42,43] have accumulated neutron data and demonstrated that the standard statistical model calculations cannot reproduce experimental pre-scission multiplicities, even at excitation energies below 100 MeV.[44] This enhancement of neutron emission before the scission point has been treated either as an increase of the nuclear viscosity which increases the saddle-to-scission time scale[45] or as a longer transition time to reach the saddle-point deformation.[46] As pointed out by Hilscher *et al.*,[47] at high excitation energies the time needed to cool the hot nucleus by particle evaporation can be comparable to or shorter than the time needed to fission. The starting point of these models is to take into account the relaxation times of the collective nuclear degrees of freedom to allow more neutron emission before the scission. They assume that all degrees of freedom for the hot nucleus are equilibrated except the deformation. The dynamical ingredients are then introduced by the dissipative coupling of the fission degree of freedom and the thermal excitation energy (nuclear friction constant, nuclear viscosity).

Our results have been compared with dynamic calculations of Delagrange *et al.*[48] where the fission process is described with a diffusion equation involving the elongation degree of freedom. A generalized form of a Fokker-Planck equation is used to follow the time evolution of the hot nucleus. This formalism takes account of the change of temperatures during the evaporation and also

TABLE II. Comparisons of the experimental pre-scission multiplicities with the statistical codes PACE2 and CASCADE and with dynamical calculations.

	$E_x=251$ MeV			$E_x=293$ MeV		
Particle	n	p	α	n	p	α
Data	6.1±1.5	0.51±0.07	0.48±0.07	8.5±1.6	0.70±0.08	0.75±0.08
PACE2	1.6	0.33	0.25	1.90	0.37	0.30
CASCADE	1.4	0.35	0.31	1.8	0.40	0.45
Dynamical calculations	7.9	2.9	0.70	8.8	3.6	0.86

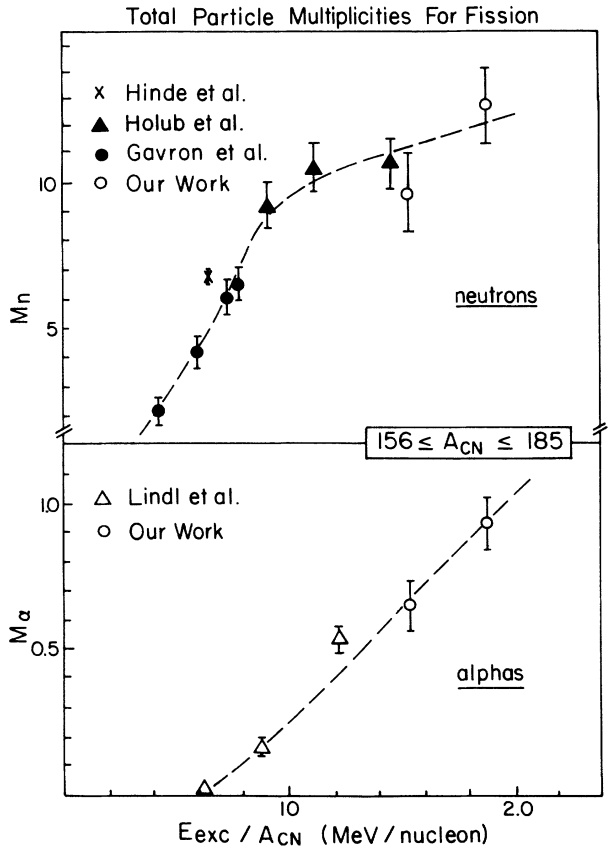

FIG. 22. Total neutron and α-particle multiplicities for fission versus the excitation energy per nucleon. Data of Holub *et al.* (Ref. 43), Gavron *et al.*, (Ref. 42) and Lindl *et al.* (Ref. 36) are also plotted. The lines are guide lines.

has the advantage of including the charged-particle emission in competition with neutron evaporation and fission. The model is fully described in Ref. 48. The calculations have been further improved by using a more realistic description of the dependence of the fission barrier with the temperature.[49] The calculated multiplicities are contained in Table II. In Fig. 23 we present our pre-scission neutron multiplicities versus the excitation energies together with previous results of Gavron *et al.*[42] and Hinde *et al.*[50] performed at lower bombarding energies. The dot-dashed line represents the dynamical calculations for the composite system ^{160}Yb. The parameters associated with ^{160}Yb and decay daughter nuclei in the de-excitation cascade were used for the ^{158,156}Er de-excitation cascade. Within experimental uncertainties, the dynamical calculations agree with the pre-scission neutron multiplicities over a wide range of excitation energy. For the α-particle case, the calculations give 0.70 and 0.86 at 251 and 293 MeV excitation energies, respectively, which may be compared with our experimental multiplicities 0.48 ± 0.07 and 0.75 ± 0.08. The calculations overpredict the proton multiplicities, giving values of 2.9 and 3.6 for the two energies, respectively, while the measurements give multiplicities of 0.51 ± 0.07 and 0.70 ± 0.08. This discrepancy may arise from an oversimplified treatment of the transmission coefficients and of the angular momentum effects.

We note, as pointed out by Delagrange *et al.*, that this model should be considered as a first step in the description of heavy-ion collisions. The elongation degree of freedom introduced in the formalism does not account, for instance, for oscillations or vibrations of the nuclear shape. Nevertheless, the viscosity coefficient associated with the motion of the collective variable should simulate the fact that dissipative phenomena take place. In Sec. III B we have investigated microscopic approaches for the central collision by solving the VUU equation. The damping of the compression-extension modes in these calculations is dominated by the mean-field effect including some two-body collision corrections. As long as the mean field is dominant, this one-body dissipation could be simulated by introducing viscosity coefficients in macroscopic equations. In a paper of Westmeier and Esterlund,[51] a phenomenological model has reproduced prescission data by introducing the effect of nuclear vibra-

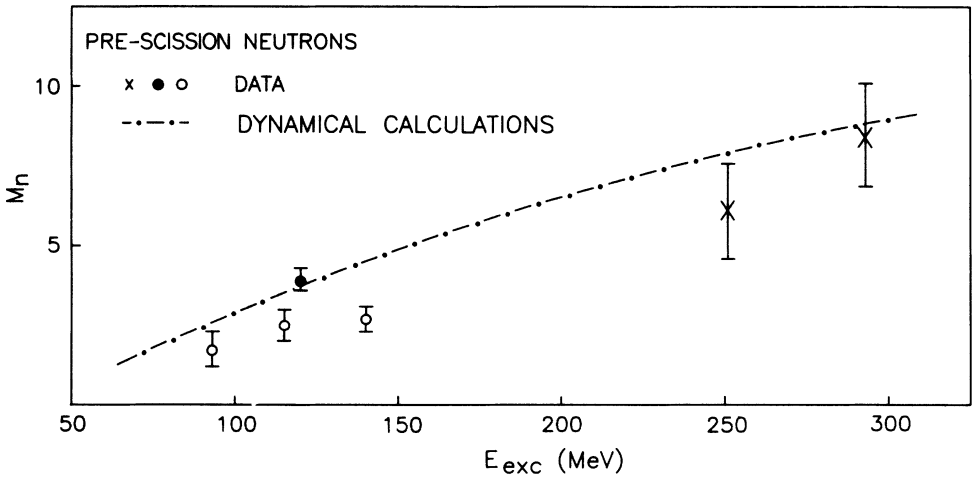

FIG. 23. Multiplicities of pre-scission neutrons versus the excitation energy of the compound nucleus. Our data (×) are compared with those of Gavron *et al.* (Ref. 42) (○) and Hinde *et al.* (Ref. 50) (●). The dot-dashed line represents dynamical calculations. See text.

tions. One important feature of this model is that the pre-scission multiplicity is assumed to be inversely proportional to the frequency of nuclear β-quadrupole vibration.

Even though the VUU calculations do not include the fission barriers, this model gives results at higher impact parameters which might be compared with our fissionlike data. For instance, we performed calculations at 10.9 MeV bombarding energy for peripheral collisions ($b = 8$ fm, $l \simeq 180\hbar$) corresponding to a fast-fission process or a fully damped deep-inelastic process. For this impact parameter, the VUU calculations predict that the composite system has emitted 12.0 particles before splitting into two fragments at 500 fm/c (1.65×10^{-21} s). Our data gave $\simeq 9$ particles (neutrons+protons, see Table II) for the pre-scission multiplicity at this bombarding energy.

V. COMPARISON OF LIGHT PARTICLE EMISSION IN COINCIDENCE WITH EVAPORATION RESIDUES AND FISSIONLIKE FRAGMENTS

In order to further characterize the hot nucleus, we may compare the particle emission produced in the evaporation residue channel and in the fissionlike channel. These two de-excitation processes of the hot nucleus are characterized by different average angular momenta. By selecting different spins, we may select different equilibrated shapes for the hot nuclei. The liquid-drop models have shown that the deformation of the nucleus increases with its spin due to the centrifugal effects. The comparisons of the apparent temperatures, emission Coulomb barriers, and multiplicities at the two bombarding energies are summarized in Fig. 24. The energy balance dia-

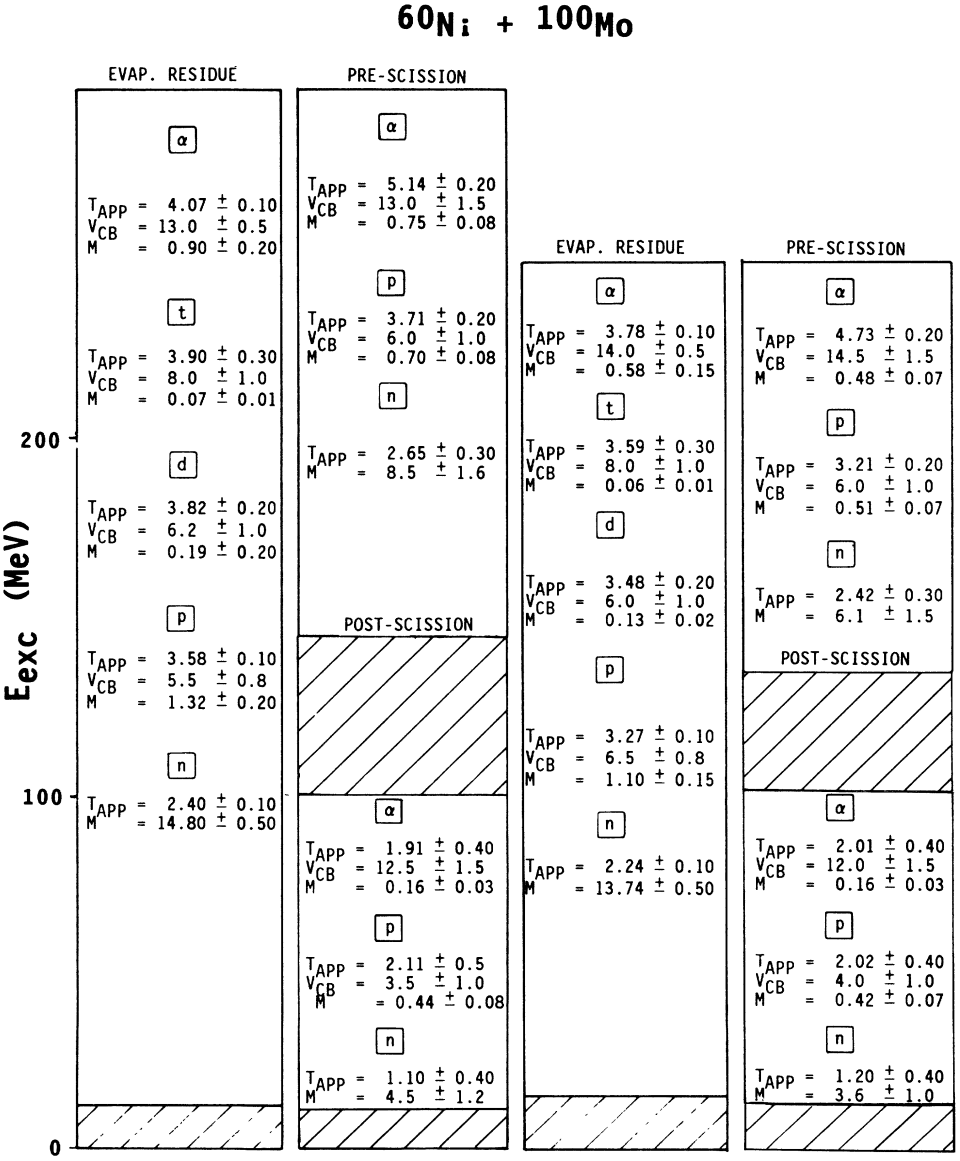

FIG. 24. Particle multiplicities, temperatures, and barriers for particles observed in fusion-evaporation and fusion-fission channels. Vertical scale corresponds to excitation energy. Hatched areas represent energy not accounted for by particle emission. See text for discussion.

grams are presented. The hatched regions represent the unaccounted for energy, i.e., γ-ray energy and the value (Q −TKE) in the fission channel.

For rapidly rotating nuclei the mean energy of the light particle spectrum is expected to be increased. This energy enhancement, which has been termed spin-off energy,[52] depends on the moment of inertia of the nucleus, its temperature, its spin, and the mass of the emitted particle. This spin-off energy modifies the slope and therefore the apparent temperatures of the spectrum. Ajitanand *et al.*[52] have described a method to estimate this effect. In the fusion-evaporation channel, the effect on the observed temperatures is negligible for the proton and neutron emission. For the α-particle emission, the increase of the observed slope reaches only a few percent. For the fusion fission, the spin-off effect does not exceed the magnitude of the error bars for the proton and neutron emission. In contrast and as expected, α-particle data are more sensitive to the spin of the emitter nucleus. As shown in the histogram, we observed a difference between the apparent temperatures for α particles measured in coincidence with evaporation residues and fission fragments of 0.95±0.22 MeV and 1.07±0.22 MeV at 251 and 293 MeV excitation energies, respectively. If we assume $140\hbar$ for the average spin of the emitter and an axis ratio of 1.5/1 comparable to those observed in the VUU calculations, the calculation gives 0.91 MeV for the spin-off energy. This is in agreement with the data, and indicates that the intrinsic temperatures are the same for α emission in the two reaction channels. Note, however, that the calculation was done assuming high average spin which indicates a large contribution of the fast-fission process whose cross section we have not measured. The deformation suggests that the α-particle prefission emission occurs early in the compound nucleus de-excitation well before the saddle-to-scission transition. The observation of the same apparent temperatures (corrected by the spin-off effect) and multiplicities (within experimental errors) for fission and evaporation residue for the α particles supports our previous conclusion that the emission probability of α particles occurs early in the cascade and is small below ~100 MeV excitation energies. For protons the temperatures are similar but the multiplicity observed with evaporation residues is larger than that observed in coincidence with fission. This indicates emission earlier in the cascade but over a larger excitation energy range for protons than for α particles. As can be seen in the histogram, we found the same emission barriers for α particles in both channels. This fact again indicates that the emission of the α particle occurs at the beginning of the de-excitation process where the shape of the nucleus which eventually fissions is close to the shape of the nucleus which does not. In the proton case, we observed the same behavior.

For the neutron emission we find only a slightly higher apparent temperature in the fission channel, which is more surprising and puzzling. This trend was also observed in previous works.[43] To estimate the temperature expected for the pre-scission emission, we have generated a total neutron spectrum by summing spectra over the neutron cascade. At each step, the variation of the level density parameter a has been taken into account. The relative contribution to the total spectrum has been calculated based on our multiplicities and on results of Refs. 42, 43, and 50. We found an average temperature of 2.6 MeV for the whole cascade at 293 MeV excitation energy. By generating the spectrum of the neutron cascade at excitation energies above 140 MeV, we found an average temperature of 3.9 MeV. Figure 24 shows that the results for the neutron temperatures are not consistent with this simulation. This behavior might reflect a different level density parameter a in fusion fission and fusion evaporation. The ratio of the parameter a between the saddle-point shape and spherical shape of the nucleus can be estimated following the treatment of the level density by Töke and Swiatecki[53] using a diffuse surface region for the Fermi-gas model. Nevertheless, even by taking strong deformed saddle-point shape (touching spheres), the change of a appears to be too small to explain the change in the neutron pre-scission temperatures.

Finally, we note the consistency of the total multiplicity for the light particle emission in the evaporation residue channel with the experimental masses of the evaporation residues (Fig. 6) which emphasizes the absence of any significant fragment emission.

VI. SUMMARY

In this paper, we have presented data on the emission of neutrons and charged particles observed in coincidence with fission fragments and evaporation residues produced in the reaction ^{60}Ni+^{100}Mo. The compound nucleus has been formed at 251 and 293 MeV excitation energies.

An analysis of the particle spectra for the evaporation residue channel shows the same initial temperatures for each kind of evaporated particle providing strong evidence for statistical equilibrium in the hot nucleus. The level density parameter a reaches a value of $A/13.8$ MeV^{-1}, confirming the decrease of this parameter at high excitation energies. The apparent temperatures and multiplicities resulting from the de-excitation cascade reflect a preferential emission for the charged particle during the first steps of the decay chain corresponding to an emission threshold near $\simeq$100 MeV excitation energy.

In the fission channel, a saturation of the post-scission emission with increasing excitation energy appears between 130 and 160 MeV excitation energy. An energy balance estimated by the multiplicities and the average kinetic energies removed during the particle evaporation indicate that the scission occurs close to 140 MeV excitation energy. The data also suggest that the pre-scission α-particle emission occurs during the first steps of the de-excitation cascade. For the α-particle energy spectra, angular momentum effects have been observed (and corrected) by comparing the apparent temperatures extracted in the fission channel with those extracted in the evaporation residue channel.

Statistical calculations are not able to describe the overall set of experimental data. Including an *ad hoc* empirical low-energy emission threshold for the charged-particle emission gives better agreement with the apparent temperatures and multiplicities in the evaporation

residue channel. Nevertheless, it is stressed that the role of dynamical effects like compression-extension modes in the "quasi-first-chance" emission spectra cannot be simulated by adjusting the standard parameters in these statistical models. Microscopic calculations (VUU) have shown how the damping time of collective motions could be longer than the lifetime of the hot nucleus for excitation energies near 2 MeV/nucleon. The enhancement of prefission multiplicities has also required dynamical calculations based on the relaxation time for collective variables. Reasonable agreement between experimental data and this model has been found but discrepancies in the charged-particle multiplicities indicate that even more sophisticated models are required for the de-excitation of hot nuclei.

ACKNOWLEDGMENTS

We thank H. Delagrange and C. Grégoire for providing the pre-scission calculations. We thank B. Glagola and the Atlas operation crew for the excellent support during our run. This work was supported by the Department of Energy under Grant DE-FG05-86ER40256 and by The Robert A. Welch Foundation and supported in part by the Bundesministerium für Forschung (BMF) and Gesellschaft für Schwerionenforschung (GSI) Darmstadt.

[1]See, e.g., *Proceedings of The Texas A&M Symposium on Hot Nuclei,* edited by S. Shlomo, R. P. Schmitt, and J. B. Natowitz (World Scientific, Singapore, 1988).

[2]B. Fornal, M. Gonin, G. Nebbia, G. Prete, G. Viesti, R. Wada, Y. Lou, K. Hagel, L. Cooke, P. Gonthier, M. Gui, G. Nardelli, R. P. Schmitt, B. Srivastava, W. Turmel, D. Utley, H. Utsunomiya, B. Wilkins, R. Zanon, and J. B. Natowitz, in Proceedings of Oaxtepec Conference on Nuclear Physics, Oaxtepec, Mexico, 1989, edited by E. Belmont and A. Menchaca-Rocha (unpublished).

[3]H. A. Weidenmüller, Nucl. Phys. **A471**, 1c (1987).

[4]M. Gonin, L. Cooke, K. Hagel, Y. Lou, J. B. Natowitz, R. P. Schmitt, B. Srivastava, W. Turmel, H. Utsunomiya, R. Wada, B. Fornal, G. Nardelli, G. Nebbia, G. Viesti, R. Zanon, G. Prete, P. Gonthier, and B. Wilkins, Phys. Lett. B **217**, 406 (1989).

[5]H. Neidel, H. Henschel, G. Geissel, and T. Laichter, Nucl. Instum. Methods **212A**, 299 (1983).

[6]M. Ogihara, Y. Nagashima, W. Galster, and T. Mikumo, Nucl. Instrum. Methods **251A**, 313 (1986).

[7]M. Anghinolfi, G. Ricco, P. Corvisiero, and F. Masulli, Nucl. Instrum. Methods **165**, 217 (1979).

[8]J. B. Natowitz, S. Leray, R. Lucas, C. Ngô, E. Tomasi, and C. Volant, Z. Phys. A **325**, 467 (1986).

[9]H. Morgenstern, W. Bohne, W. Galster, K. Grabisch, and A. Kyanowski, Phys. Rev. Lett. **52**, 1105 (1984); G. S. F. Stephans, D. G. Kovar, R. V. F. Janssens, G. Rosner, H. Ikezoe, B. Wilkins, D. Henderson, K. T. Lesko, J. J. Kolata, C. K. Gelbke, B. V. Jacak, Z. M. Koenig, G. D. Westfall, A. Szanto de Toledo, E. N. Dzanto, and P. L. Gonthier, Phys. Lett. **161B**, 60 (1985).

[10]R. Trockel, K. D. Hildenbrand, U. Lynen, W. F. J. Müller, H. J. Rabe, H. Sann, H. Stelzer, W. Trautmann, R. Wada, E. Eckert, P. Kreutz, A. Kühmichel, and J. Pochodzalla, Phys. Rev. C **39**, 729 (1989).

[11]R. Wada, D. Fabris, K. Hagel, G. Nebbia, Y. Lou, M. Gonin, J. B. Natowitz, R. Billerey, B. Cheynis, A. Demeyer, D. Drain, D. Guinet, C. Pastor, J. Alarja, A. Giorni, D. Heuer, C. Morand, B. Viano, C. Mazur, C. Ngô, S. Leray, R. Lucas, M. Ribrag, and E. Tomasi, Phys. Rev. C **39**, 497 (1989).

[12]W. Dilg, W. Schantl, H. Vonach, and M. Uhl, Nucl. Phys. **A217**, 269 (1973).

[13]G. Nebbia, K. Hagel, D. Fabris, Z. Majka, J. B. Natowitz, R. P. Schmitt, B. Sterling, G. Mouchaty, G. Berkowitz, K. Strozewski, G. Viesti, P. L. Bonthier, B. Wilkins, M. N. Namboodiri, and H. Ho, Phys. Lett. B **176**, 20 (1986).

[14]K. Hagel, D. Fabris, P. Gonthier, H. Ho, Y. Lou, Z. Majka, G. Mouchaty, M. N. Namboodiri, J. B. Natowitz, G. Nebbia, R. P. Schmitt, G. Viesti, R. Wada, and B. Wilkins, Nucl. Phys. **A486**, 429 (1988).

[15]A. Lejeune, P. Grange, M. Martzolff, and J. Cugnon, Nucl. Phys. **A453**, 189 (1986).

[16]D. Vautherin and N. Vinh Mau, Orsay Report/PNO/TH 87-03, 1987; N. Vinh Mau, Orsay Report/PNO/TH 87-81, 1987; S. Shlomo and J. B. Natowitz, Progress Report, Cyclotron Institute, Texas A&M University, 1987–1988 (unpublished).

[17]R. W. Hasse and P. Schuck, Phys. Lett. B **179**, 189 (1986); P. F. Bortignon and C. H. Dasso, *ibid.* **189**, 381 (1987).

[18]W. E. Parker, M. Kaplan, D. J. Moses, G. La Rana, D. Logan, R. Lacey, J. M. Alexander, D. M. de Castro Rizzo, P. De Young, R. J. Welberry, and J. T. Boyer (submitted to Phys. Rev. C).

[19]G. F. Peaslee, N. N. Ajitanand, J. N. Alexander, R. Lacey, L. C. Vaz, M. Kaplan, M. Kildir, D. J. Moses, D. Logan, and M. S. Zisman, Phys. Rev. C **39**, 488 (1989), and references therein.

[20]F. Pühlhofer, Nucl. Phys. **A280**, 267 (1977).

[21]J. M. Alexander, G. Auger, M. Kaplan, L. Kowalski, R. Lacey, G. La Rana, M. T. Magda, and G. F. Peaslee, in Proceedings of the Dallas Symposium on Nuclear Dynamics and Nuclear Disassembly, 1989, edited by J. B. Natowitz (unpublished).

[22]K. Hagel, Ph.D. thesis, Texas A&M University, 1986.

[23]A. Gavron, Phys. Rev. C **20**, 230 (1980).

[24]R. K. Choudhury, P. L. Gonthier, K. Hagel, M. N. Namboodiri, J. B. Natowitz, L. Adler, S. Simon, S. Kniffen, and G. Berkowitz, Phys. Lett. **143B**, 74 (1984).

[25]J. R. Huizenga and G. Igo, Nucl. Phys. **29**, 462 (1962).

[26]S. Cohen, F. Plasil, and W. J. Swiatecki, Ann. Phys. (N.Y.) **82**, 557 (1974).

[27]V. Strutinski, Nucl. Phys. **A122**, 1 (1968).

[28]M. Brack and Ph. Quentin, Phys. Lett. **52B**, 159 (1974).

[29]K. Niita, W. Cassing, and U. Mosel, Nucl. Phys. **A504**, 391 (1989).

[30]G. Sauer, H. Chandra, and M. Mosel, Nucl. Phys. **A269**, 221 (1976).

[31]P. Bonche, S. Levit, and D. Vautherin, Nucl. Phys. **A436**, 265 (1985).

[32]S. Shlomo (unpublished).

[33]V. E. Viola, K. Kwiatkowski, and M. Walker, Phys. Rev. C

31, 1550 (1985).
[34]E. Duek, N. N. Ajitanand, J. M. Alexander, D. Logan, M. Kildir, L. Kowalski, L. C. Vaz, D. Guerreau, M. S. Zisman, and M. Kaplan, Phys. Lett. **131B**, 297 (1983).
[35]J. M. Miller, G. L. Catchen, D. Logan, N. Rajagopalan, J. M. Alexander, M. Kaplan, and M. S. Zisman, Phys. Rev. Lett. **40**, 100 (1978).
[36]B. Lindl, A. Brucker, M. Bantel, H. Ho, R. Muffler, L. Schad, M. G. Trauth, and J. P. Wurm, Z. Phys. A **328**, 85 (1987).
[37]R. Vandenbosch and R. Huizenga, *Nuclear Fission* (Academic, New York, 1973).
[38]N. Cârjan and B. Leroux, Phys. Rev. C **22**, 2008 (1980).
[39]M. Gonin, L. Cooke, B. Fornal, P. Gonthier, M. Gui, Y. Lou, J. B. Natowitz, G. Nardelli, G. Nebbia, G. Prete, R. P. Schmitt, B. Srivastava, W. Turmel, D. Utley, H. Utsunomiya, G. Viesti, R. Wada, B. Wilkins, and R. Zanon, Nucl. Phys. **A495**, 139 (1989).
[40]D. Hilscher, H. Rossner, B. Cramer, B. Gebauer, U. Jahnke, M. Lehrmann, E. Schwinn, M. Wilpert, Th. Wilpert, H. Frobeen, E. Nordhorst, and W. Scobel, Phys. Rev. Lett. **62**, 1099 (1989).
[41]A. J. Sierk, Phys. Rev. C **33**, 2039 (1986).
[42]A. Gavron, A. Gayer, J. Boissevain, H. C. Britt, T. C. Awes, J. R. Beene, B. Cheynis, D. Drain, R. L. Ferguson, F. E. Obenshain, F. Plasil, G. R. Young, G. A. Petitt, and C. Butler, Phys. Rev. C **35**, 579 (1987).
[43]E. Holub, D. Hilscher, G. Ingold, U. Jahnke, H. Orf, and H. Rossner, Phys. Rev. C **28**, 252 (1983).
[44]D. J. Hinde, R. J. Charity, G. S. Foote, J. R. Leigh, J. O. Newton, S. Ogaza, and A. Chatterjee, Nucl. Phys. **A452**, 550 (1986).
[45]J. R. Nix, A. J. Sierk, H. Hofmann, F. Scheuter, and D. Vautherin, Nucl. Phys. **A424**, 239 (1984).
[46]P. Grange and H. A. Weidenmüller, Phys. Lett. **96B**, 26 (1980).
[47]D. Hilscher, D. J. Hinde, and H. Rossner, *Proceedings of The Texas A&M Symposium on Hot Nuclei* (World Scientific, Singapore, 1988).
[48]H. Delagrange, C. Gregoire, and F. Scheuter, Z. Phys. A **323**, 437 (1986).
[49]C. Guet, E. Strumberger, and M. Brack, Phys. Lett. B **205**, 427 (1988).
[50]D. J. Hinde, H. Oyata, M. Tanaka, T. Shimoda, N. Takahashi, A. Shinohara, S. Wakamatsu, K. Katori, and H. Okamura, Phys. Rev. C **39**, 2268 (1989).
[51]W. Westmeier and R. A. Esterlund, Z. Phys. A **316**, 27 (1989).
[52]N. N. Ajitanand, G. La Rana, R. Lacey, J. Moses, L. C. Vaz, G. F. Peaslee, D. M. de Castro Rizzo, M. Kaplan, and J. Alexander, Phys. Rev. C **34**, 877 (1986), and references therein.
[53]J. Töke and W. J. Swiatecki, Nucl. Phys. **A372**, 141 (1981).